Journal of Medicinal Chemistry

Brief Article

(S)-2-Amino-3-(5-methyl-3-hydroxyisoxazol-4-yl)propanoic Acid (AMPA) and Kainate Receptor Ligands: Further Exploration of Bioisosteric Replacements, Structural and Biological Investigation

Simone Brogi, Margherita Brindisi, Stefania Butini, Giridhar Uttam Kshirsagar, Samuele Maramai, Giulia Chemi, Sandra Gemma, Giuseppe Campiani, Ettore Novellino, Paolo Fiorenzani, Jessica Pinassi, Anna Maria Aloisi, Mikko Gynther, Raminta Venskutonyte, Liwei Han, Karla Frydenvang, Jette Sandholm Kastrup, and Darryl S. Pickering

J. Med. Chem., **Just Accepted Manuscript** • DOI: 10.1021/acs.jmedchem.8b00099 • Publication Date (Web): 16 Feb 2018

ACS Publications

Journal of Medicinal Chemistry is published by the American Chemical Society. 1155 Sixteenth Street N.W., Washington, DC 20036

(*S*)-2-Amino-3-(5-methyl-3-hydroxyisoxazol-4-yl)propanoic Acid (AMPA) and Kainate Receptor Ligands: Further Exploration of Bioisosteric Replacements, Structural and Biological Investigation

Simone Brogi,[¶] Margherita Brindisi,[¶] Stefania Butini,[¶,*] Giridhar U. Kshirsagar,[¶] Samuele Maramai,[¶] Giulia Chemi,[¶] Sandra Gemma,[¶] Giuseppe Campiani,[¶,*] Ettore Novellino,[∫] Paolo Fiorenzani,[#] Jessica Pinassi,[#] Anna Maria Aloisi,[#] Mikko Gynther,[▽] Raminta Venskutonytė,[⊥] Liwei Han,[⊥] Karla Frydenvang,[⊥] Jette Sandholm Kastrup,[⊥,*] Darryl S. Pickering[⊥,*]

[¶]Department of Biotechnology, Chemistry and Pharmacy, NatSynDrugs, University of Siena, via A. Moro 2, 53100 Siena, Italy; [∫]Department of Pharmacy, University of Napoli Federico II, via D. Montesano 49, 80131, Napoli, Italy [#]Department of Medicine, Surgery and Neuroscience, University of Siena, viale M. Bracci 16, 53100 Siena, Italy; [▽]School of Pharmacy, Faculty of Health Sciences, University of Eastern Finland, 70211 Kuopio, Finland; [⊥]Department of Drug Design and Pharmacology, University of Copenhagen, Jagtvej 162, DK-2100 Copenhagen, Denmark.

KEYWORDS. Kainate receptors, binding pharmacology, crystallography, computational modeling, inflammatory pain

ABSTRACT: Starting from **1-4** and **7** structural templates, analogues based on bioisosteric replacements (**5a-c** *vs* **1**, **2** and **6** *vs* **7**) were synthesized for completing the SAR analysis. Interesting binding properties at GluA2, GluK1 and GluK3 receptors were discovered. The requirements for GluK3 interaction were elucidated determining the X-ray structures of the GluK3-LBD with **2** and **5c** and by computational studies. Antinociceptive potential was demonstrated for GluK1 partial agonist **3** and antagonist **7** (2 mg/kg ip).

Introduction

L-Glutamate (*L*-Glu) mediates most of the fast excitatory synaptic signaling in the central nervous system (CNS) by means of heteromeric ligand-gated ion channels (ionotropic *L*-Glu receptors, iGluRs).[1] Kainate receptors (KARs) are, together with (*S*)-2-amino-3-(5-methyl-3-hydroxyisoxazol-4-yl)propanoic acid (AMPA) and *N*-methyl-*D*-aspartate receptors, tetrameric ligand-gated ion channels. All the identified KAR (GluK1-5) subunits can combine *in vitro* to form heteromeric receptors,[1,2] likely in a dimer-of-dimers topology.[3] KARs are distributed in various areas of the CNS;[4] they are localized on both pre- and postsynaptic cell membranes contributing to fast excitatory signaling and synaptic plasticity. Among iGluRs, GluA2, GluK1 and GluK3 subtypes are implicated in various neurological diseases such as depression, pain, neurodegeneration, and epilepsy; though their normal physiological function is not fully understood yet.[5-7] Nociception (the sensorial input mainly travelling through the spinothalamic tract) and pain (the conscious aspect) are supported by ascending and descending pathways. Nociception propagates to the dorsal horn of the spinal cord, through the cell soma residing in the dorsal root ganglion (where GluK1 receptors are widely expressed) and is sent to the cortex for higher-order processing (pain). From the brain, descending pathways travel towards the spinal cord. These pathways may produce analgesic effects by stimulation of opioid receptors and by modulation of the GABAergic tone on the nociceptive dorsal horn neurons.[8] Further, the presynaptic GluK1 receptors are also relevant to the supraspinal pain pathways as it has been demonstrated that GluK1 inhibition can attenuate, among others, the spinothalamic signaling to the thalamus.[8] GluK1 relevance as therapeutic targets in this field was assessed by a number of animal studies, mainly in models of chronic pain, where KARs inhibition or their genetic ablation was effective in reducing the pain behaviors. Small clinical trials were also performed using several orthosteric antagonists.[8]

Chart 1. Reference compounds (1-4 and 7) and title compounds 5a-c and 6.

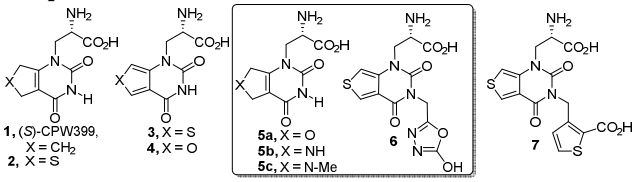

With the specific aim to extend our previous work and explore novel bicyclic pyrimidinedione-based compounds typified by **1**[9] and its analogues **2**,[10] **3**[10] and **4**[11] (Chart 1), and to investigate GluK3 interaction with ligands, the five membered fused system was modified in compounds **5a-c** for completing the structure-activity relationship (SAR) analysis of bioisosteric-replacements at the five membered system. Further, our GluK1 antagonist **7** inspired the development of derivative **6** (Chart 1). The 2-hydroxyoxadiazole system was used as a potential bioisosteric alternative[12] to the thiophene-2-carboxylate system of **7**[11] (Fig. S1).

RESULTS AND DISCUSSION

Chemistry. The chemistry for **5a-c** and **6** is reported in Schemes 1-3. For **5a-c** (Schemes 1, 2) *β*-keto esters **9**[13] and **15**[14,15] were needed for the synthesis of the key pyrimidinediones **12**, **20** and **21**. After *N*1 alkylation of these latter compounds and Boc deprotection of the amino acidic lateral chain **5a-c** were obtained. For the synthesis

of **6** (Scheme 3) cyclization of the ureido derivative **24** gave the pyrimidinedione **25** which underwent *N*1 alkylation (for a more detailed description please refers to the Supporting Information, SI).

Scheme 1. Synthesis of 5a[a]

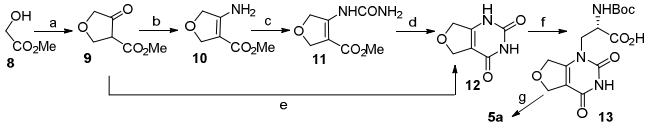

[a]Reagents and conditions: (a) NaH, Et_2O, 1 h, then methyl acrylate, DMSO, 0 °C, 1 h, then rt, 5 h, 81%; (b) NH_4OAc, EtOH, reflux, 12 h, 32%; (c) phosgene 20% in toluene, pyridine, 1,2-dichloroethane, 0 °C, 3 h, then NH_4OH, reflux, 13 h, 19%; (d) MeONa, MeOH, rt, 12 h, 52%; (e) urea, conc. HCl, MeOH, reflux, 2 h, then 2 N NaOH, H_2O, reflux 1.5 h, 45%; (f) NaH, DMF, rt, 2 h, then -65 °C (*S*)-*N*-Boc-3-amino-2-oxetanone, rt, 14 h, 8%; (g) TFA, DCM, rt, 4 h, 35%.

Scheme 2. Synthesis of 5b,c[a]

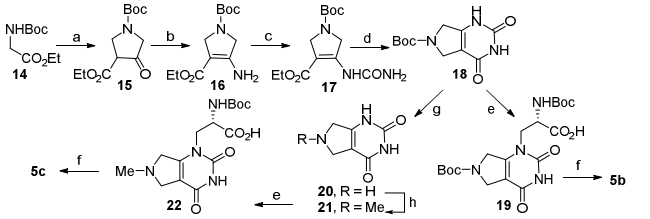

[a]Reagents and conditions: (a) NaH, ethyl acrylate, toluene, 0 °C, 0.5 h then, 60 °C, 4 h, 50%; (b) NH_4OAc, EtOH, reflux, 12 h, 90%; (c) phosgene 20% in toluene, pyridine, 1,2-dichloroethane, 0 °C, 3 h, then NH_4OH, reflux, 13 h, 80%; (d) EtONa, MeOH, rt, 12 h, 77%; (e) NaH, DMF for **19**, DMF/DMSO for **22**, rt, 2 h, then -65 °C (*S*)-*N*-Boc-3-amino-2-oxetanone, rt, 14 h, 9% for **19** and 29% for **22**; (f) TFA, DCM, rt, 4 h, 80% for **5b** and 50% for **5c**; (g) HCl, MeOH, 0 °C, 0.5 h then, rt, 3 h, 91%; (h) formaldehyde, $NaBH(OAc)_3$, EtOH, 13 h, 45%.

Scheme 3. Synthesis of 6[a]

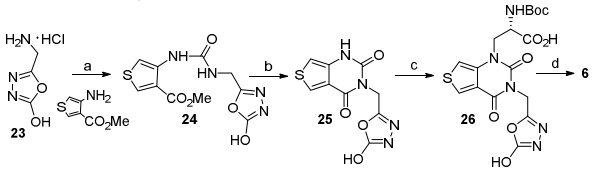

[a]Reagents and conditions: (a) methyl 4-aminothiophene-3-carboxylate, triphosgene, toluene, reflux, 3 h, then **24**, rt, 13 h, 34%; (b) MeONa, MeOH, rt, 12 h, 93%; (c) NaH, DMF, rt, 2 h, then -65 °C, (*S*)-*N*-Boc-3-amino-2-oxetanone, rt, 14 h, 3%; (d) TFA, DCM, rt, 4 h, 42%.

Table 1. Binding affinities at recombinant homomeric rat AMPA receptors and KARs expressed in *Sf9* cells.

	K_i (μM)				Selectivity	
Cmpds	GluA2	GluK1	GluK2	GluK3	GluK3/ GluK1	GluK3/ GluA2
1[9]	0.223± 0.012	0.044± 0.004	>1000	5.09± 1.19	116	23
2[10]	0.080± 0.013	0.0052±0.0003	>1000	3.25± 0.30	625	41
3[10]	0.465± 0.002	0.0039± 0.0004	>1000	1.02± 0.25	262	21
4[11]	44 ± 4	2.98 ± 0.52	>1000	> 1000	> 336	23
5a	0.331± 0.058	0.586 ± 0.116	>1000	111 ± 26	190	336
5b	2.37 ± 0.21	0.869 ± 0.063	>1000	18.1 ± 1.7	21	8
5c	1.99 ± 0.57	0.356 ± 0.023	>1000	2.15± 0.10	6	1
6	> 100	36 ± 3	>1000	≈ 100	> 3	-
7[11]	73 ± 15	0.157 ± 0.022	99 ± 22	7.45± 0.30	47	0.1

Mean ± SEM of at least three competition experiments at 12-16 drug concentrations performed in triplicate.

***In vitro* Activity**. Compounds **5a-c** displayed micromolar affinities at GluA2, GluK1 and GluK3 subunits (Table 1). They also displayed from good to moderate selectivity for GluK1 over GluK2, GluK3 and GluA2 with the exception of **5a** which displayed a higher affinity for GluA2 (K_i GluA2 = 0.331 μM) than **5b** (K_i GluA2 = 2.37 μM) and **5c** (K_i GluA2 = 1.99 μM). It is noteworthy that while analogues **5b** and **5c** displayed comparable affinity at GluK1 their affinity towards GluK3 differed by at least one order of magnitude, while **5a** was found to have K_i > 100 μM at GluK3. The order of affinity at AMPA receptors and KARs follows the trend GluK1>GluA2>GluK3 (for **5b,c**) and GluA2>GluK1>GluK3 (for **5a**). The pharmacological profile of **5a** substantially differs from that of its furan-based analogue (**4**). **4**, compared to the other compounds, has a lower affinity at GluA2 and GluK1[11] and is inactive at inactive at GluK2 and GluK3 receptors. This observation prompted an in-depth computational analysis, as discussed below. By this series of ligands we observed that the introduction of nitrogen in the pyrimidinedione-fused system was the best choice to maintain GluK3 affinity while lowering GluK1 and GluA2 affinity compared to the other ligands. Accordingly, **5c** was identified as the most promising ligand for the study of the GluK3 receptor subtype. Compound **6**, with a structure inspired by our antagonist **7**,[11] resulted a weak GluK1 ligand. We assume that the observed low affinity is due to the short length of the (mono-methylene) side-chain spacing the 1,3,4-oxadiazole subunit from the pyrimidinedione system. This may hamper the acidic proton from perfectly overlapping the position occupied by the carboxylate moiety of our lead compound **7**. Accordingly, the hydroxyl functionality may fail to establish suitable contacts within the ligand-binding domain (LBD) of the target receptors as observed by molecular modeling studies (not shown).

X-ray Crystallography. X-ray crystallography was used to investigate structural requirements for GluK3 ligands. The two ligands with highest affinity at GluK3, **2** and **5c**, were crystallized in complex with GluK3-LBD. The selection criteria were based on *in vitro* potency (**5c**) while **2** was selected on the basis of structural similarity to the previously developed compounds. The structure of GluK3-LBD with **2**, determined at 2.6 Å resolution, contains one molecule of GluK3-LBD in the asymmetric unit of the crystal (Table S1). The structure of GluK3-LBD with **5c**, determined at 2.4 Å resolution, contains two molecules of GluK3-LBD in the asymmetric unit of the crystal. Both structures correspond to GluK3-LBD in its monomeric form (Fig. 1A). **2** and **5c** interact in a similar way with the LBD residues (Fig. 1B-C). The α-carboxylate of the ligands forms H-bonds with the side-chain guanidino group of Arg525 (GluK3 numbering according to UNP GRIK3_RAT P42264) and the backbone nitrogen atoms of Thr520 and Ala691. The α-amino group of the ligands interacts with the side-chain of Glu739, the backbone oxygen atom of Pro518 and the side-chain of Thr520. The two pyrimidinedione oxygen atoms form contacts to the backbone nitrogen atom of Thr692 and Glu739, respectively, whereas the pyrimidinedione nitrogen atom forms a contact to the side-chain hydroxyl group of Thr692. The sulfur atom in **2** and *N*-methyl part in **5c** are located in a predominantly hydrophobic region within 5 Å

of the following residues: Glu443, Phe446, Tyr491, Pro518, Asn722, Glu739, Thr742 and Tyr765 (not shown). The sulfur atom of **2** forms a contact with the side-chain of Tyr765 (Fig. 1B), whereas the *N*-methyl in **5c** is in close contact to the side-chain carboxylate of Glu443 (mol*A*; Fig. 1C) or the side-chain amide of Asn722 (mol*B*, Fig. 1D).

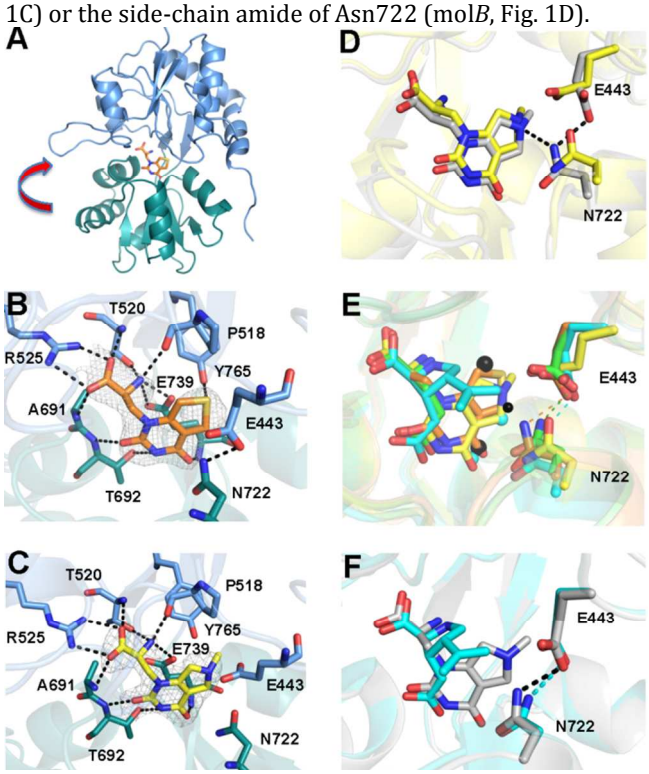

Figure 1. X-ray crystal structures of GluK3-LBD with **2** and **5c** (PDB-codes 6F29 and 6F28, respectively). (A) Cartoon representation of GluK3-LBD in complex with **2** (sticks, with C in orange, N in blue, O in red and S in yellow), lobe D1 in light blue and lobe D2 in dark green. The arrow indicates D1-D2 domain closure. (B) Binding site interactions with **2**. Polar contacts (up to 3.2 Å (except from the ligand to Thr692: 3.4 Å); black stippled lines) between binding-site residues and **2** are shown. A simple PHENIX omit 2Fo-Fc map carved around **2** and contoured at 1 sigma is shown in light grey. (C) Binding site interactions with **5c** (mol*A*, sticks with yellow carbon atoms. (D) Superimposition (on D1 residues) of mol*A* and mol*B* of GluK3-LBD with **5c** to illustrate the differences in domain closure and conformation of Glu443 and Asn722. **5c** in sticks with yellow (mol*A*) and grey (mol*B*) carbon atoms. (E) Comparison of binding mode of **2**, **5c** (mol*A*), *L*-Glu (green; PDB-code 4MH5) and kainate (cyan; PDB-code 3U92, mol*A*). Proteins were superimposed on D1 residues. GluK3 residues and D1-D2 interlobe contacts are colored according to the ligands. The three water molecules belonging to the structure with *L*-Glu are shown as black spheres and the two water molecules belonging to the structure with kainate as cyan spheres. (F) Comparison of binding mode of **5c** (mol*B*) and kainate (mol*B*, cyan).

The closures of lobe D1 and D2 (named domain closure; see Fig. 1A) introduced by binding of the ligands were calculated using DynDom[16] and are relative to an antagonist-bound structure of GluK1-LBD (PDB-code 3S2V, mol*B*) as described.[17] Compound **2** induced a domain closure of 35° (Fig. 1D), similar to that induced by *L*-Glu in GluK3-LBD (without zinc ions present: 36°; PDB-code 4MH5;[18] with zinc ions present: 35-36°; PDB-code 3U93[19]). A similar, although slightly smaller, domain closure is seen in mol*A* of the GluK3-LBD structure with **5c** (33°), whereas the domain closure in mol*B* of the GluK3-LBD structure with **5c** is only 28° (Fig. 1D). Such a difference in domain closure between two GluK3-LBD molecules in the same crystal has also been observed when crystallized with kainate in presence of Zn ions (mol*A*: 32°, mol*B* 29°; PDB-code 3U92[19]). When crystallized without Zn ions, kainate induces a domain closure of 32° in GluK3-LBD (PBD-code 4E0W[20]). So, the introduction of a 5-membered ring fused to the pyrimidinedione system seems to allow a similar domain closure as *L*-Glu (Fig. 1E), but can also be stabilized in a more opened conformation (Fig. 1F). The pyrimidinedione system of **2** and **5c** acts as a bioisoster of the distal carboxylate of *L*-Glu and also displaces one water molecule (Fig. 1E). In addition, the 5-membered ring in **2** and **5c** displaces two extra water molecules. The sulfur atom of **2** and the *N*-methyl of **5c** seem to affect the important D1-D2 interlobe interaction between the side-chains of Glu443 and Asn722 (Fig. 1D,E). Whereas the interaction between Glu443 and Asn722 is slightly changed in the structure of GluK3-LBD with **2** compared to the structure with *L*-Glu, Glu443 and Asn722 are poorly defined in the structure of GluK3-LBD with **5c** and need to adopt a different conformation to avoid steric clash with the *N*-methyl of **5c**. So, the presence of the bulkier Asn772 in GluK3 compared to Ser721 in GluK1 might explain the more favorable affinity at GluK1 compared to GluK3.

Molecular Modeling. We focused our efforts to rationalize the observed differences in affinity for GluK1 and GluK3 receptors of the compounds **1-7**. A comparative analysis of GluK1 and GluK3 LBDs was performed using their X-ray structures in complex with kainate (4E0X[20] for GluK1 and 4E0W[20] for GluK3). The two LBDs are highly similar in amino-acid composition, although with crucial differences: Ser741 and Ser721 in GluK1 are replaced by more hindering Thr742 and Asn722 in GluK3. Another difference is the replacement of Ser689 (GluK1) with Ala691 (GluK3). These variations result in a different size of the binding pockets (GluK1 volume 660.7 Å^3, area 641Å^2; GluK3 volume 567 Å^3, area 520 Å^2; Fig. S2). These variations, influencing the accessible volume, can affect ligand interaction.[18,21] We performed molecular docking (the protocol was validated as detailed in SI, Figs S3,S4) in GluK1 and GluK3 LBDs to study the binding modes of our compounds. Our calculations revealed that **2** establishes similar interactions into both LBDs and targets the same residues (Fig. 2A,B). It forms a salt bridge with Arg523 in GluK1-LBD and Arg525 in GluK3-LBD as seen in its X-ray structure (Fig. 1B), while the pyrimidinedione system forms H-bonds with Thr residues (Thr518 and Thr690 in GluK1; Thr520 and Thr692 in GluK3), with the backbone of Pro516 in GluK1 and Pro518 in GluK3, Gly688 in GluK1 and Gly690 in GluK3 and with Met737 in GluK1 and Met738 in GluK3 as well as with the side-chain carboxylate of Glu738 in GluK1 and Glu739 in GluK3. Moreover, we observed H-bonds with the backbone of Ala691 in GluK3. Due to the presence of Ser689 in GluK1 in place of Ala691 in GluK3 we noted a strong network of H-bonds between **2** and GluK1. Compound **2** can form H-bonds with Ser689 (backbone and side-chain) as well as an additional polar contact with Thr690. Due to the shrinkage of GluK3-LBD

we noted a reduction in H-bonds network precluding optimal accommodation of **2** into the LBD. These little differences of accommodation observed in the docking poses may help to rationalize the differences in binding affinities of **2** at GluK1 and GluK3. Regarding **3** (Fig. S5) we obtained comparable docking results as for **2** with a reduction of the number of contacts in the GluK3-LBD. The replacement of the sulfur atom of **2** with NH and *N*-Me groups in **5b** and **5c** causes a decrease in binding affinity at GluK1 (Table 1) while **5c** shows a slightly better binding affinity at GluK3 compared to **2**. The docking of **5b** into both receptors (Fig. S6) gives similar outputs with minor differences in terms of contacts, highlighting the interaction of the NH group with Glu441 and Ser741 in GluK1 and Glu443 and Thr742 in GluK3. Docking outputs of **5c** (Fig. S7A,B) showed similar interactions of the amino-acid moiety as those described for **2**. Contrarily, the pyrimidinedione moiety of **5c** is differently accommodated into GluK1-LBD, interacting with the backbones of Thr690 and Met737, lacking the H-bond with the side-chain of Thr690. The *N* atom of the *N*-Me group establishes an H-bond with the side-chain of Ser741 (Fig. S7A). The binding mode of **5c** in GluK3-LBD (Fig. S7B) revealed interactions with Thr692 and Met738. **5a** docked in a similar manner in GluK1-LBD and GluK3-LBD established a similar pattern of interaction (Fig. S8). Hence, the docking calculations are not able to explain the favorable binding affinity of the compound against GluK1 over GluK3. Interestingly, docking of **4** into GluK1 and GluK3-LBDs revealed different binding modes. We observed that when adopting an orientation into the LBD similar to that seen for **2** and **5c** in their X-ray structures, the pyrimidinedione system of **4** is slightly twisted in an orientation that precludes key contacts in the LBD (Fig. S9). Besides these results we found, for **4**, another accommodation where the ligand is completely flipped, missing the "correct" orientation and position of H-bonding atoms for the optimal interaction within the receptor (Fig. S9). Remarkably, we got this result only for **4**. For the other analogues we found a unique and reliable cluster of docked solutions (in both receptors) where the pyrimidinedione system is, as usual, projected toward Glu441, Ser741 and Tyr764 in GluK1 and Glu443, Thr742 and Tyr765 in GluK3. Then, the undefined binding mode of **4** may provide a reason for its reduced binding affinity at GluK1 and GluK3 receptors.[22] We also estimated ligand-binding energies (ΔG_{bind}) at GluK1 and GluK3 using Prime MM/GBSA (Table S2). At GluK1 the best predicted ΔG_{bind} values were obtained for **2** and **3**, followed by other ligands that exhibited nM affinities (**1** and **5a-c**). In agreement with experimental data for **4**, the calculation also revealed that it possesses the poorest affinity at the GluK1 receptor. Interestingly, we noted that the flipped orientation showed the highest ΔG_{bind}, denoting that this orientation may contribute to a dramatic reduction in GluK1 binding affinity. A similar trend was also observed at GluK3. We noted a significant increase in ΔG_{bind} for the less active compounds such as **5a** with respect to the most active ligands. Also in this case **4** showed the lowest predicted affinity. For further substantiating the above observations, we evaluated the molecules' volume for correlating it with binding affinities.[23] Calculations were carried out using different software with diverse methods for the volume estimation (see SI). After analyzing the results (Table S2) we noted a correlation between the molecules' volume and their binding affinities. The only exception is **5c** which contains an additional carbon atom on the pyrrolidine fused system (the Me group). As expected, **4** has the lowest volume, among the tested ligands. This data allowed us to speculate that the small size of **4** may lead to two different scenarios as captured by docking calculation: (i) the compound could flip when it is already inside the receptor or (ii) during the entrance in the LBD, the compound is accommodated in a non-classical and less effective way, due to its different size, with consequent reduction in binding affinity.

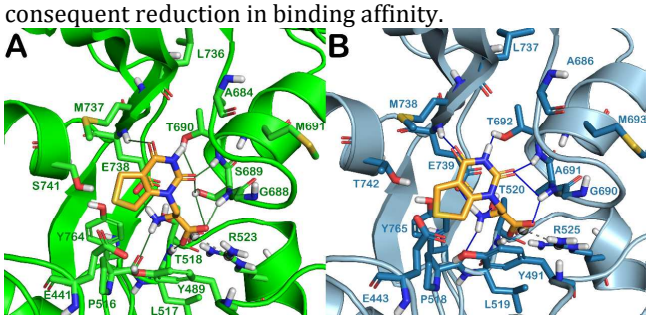

Figure 2. Representative docked poses of **2** (bright orange sticks) into GluK1-LBD (PDB-code 4E0X; green cartoon) (A) and GluK3-LBD (PDB-code 4NWC; light blue cartoon) (B). LBD residues are represented as sticks. H-bonds are represented by solid blue lines and the salt bridges as a grey dotted line between two spheres.

***In vivo* Studies.** The class of pyrimidinediones typified by CPW399 (**1**), and represented also by the analogues herein, was never investigated in animal models of pain. Thus, in order to characterize this class of GluK1 ligands, the most potent and selective analogues of the series were selected to enter into *in vivo* studies. For *in vivo* tests the GluK1 partial agonist **3** and the antagonist **7**[11] were selected and enrolled, while the new, less potent, analogs **5a-c** and **6** were not investigated.

The formalin test is a well-known method to study the behavioral response to an acute, long lasting painful stimulation.[24] The possibility to record different behavioral responses to the painful stimulation allows a deeper insight into pain mechanisms. Indeed, the time spent licking, flexing or jerking the injected paw depends on the activation of different circuits at supraspinal and/or spinal levels. Moreover, the formalin test leaves the animal free to move in a large cage, thus allowing the recording of other spontaneous, not painful responses, important for a comprehensive analysis of the drug-induced effect on the animal behavior. The formalin concentration used (5%) induced a first phase of pain behavior (10-15 min, first phase) followed by a longer lasting phase (45-50 min). The statistical analysis was carried out in the two phases separately to better determine the effects of the drugs on the first or second phase.[24] For evaluating the therapeutic potential of our GluK1 ligands in the formalin test we resynthesized compounds **3** and **7**.[11] Collected data show how **3** and **7** efficiently reduce the pain sensation already at 2 mg/kg dose i.p. (Fig. 3). The formalin-treated mice showed typical behaviors: licking, flexing, and paw jerk. These responses showed a classical biphasic time course characterized by an initial rush of pain behavior (0-15

min) followed by a second phase characterized by longer-lasting inflammatory events. The administration of **3** and **7** decreased the pain sensation as expressed by a statistically significant reduction of the pain behaviors. We flanked the classical pain-elicited behavioral observation with the locomotor activity evaluation for the same animals (Fig. S10, comparing the effect of **3** and **7** with formalin-treated and naïve groups). The general locomotor activity (walking and explorative behavior) was assessed by recording the time spent in movement for 60 min after treatment. The data revealed that in all the groups the early explorative phase usually undergoes a time-dependent decrease up to extinction. In the groups treated with **3** and **7** the initial locomotor activity paralleled that of the formalin treated animals. Interestingly, starting from 30 min of observation, the registered increase of locomotor activity nicely correlates with the analgesic profile of the tested compounds as depicted in Fig. 3. In particular, with **3** starting from 45 min of observation, the animals, almost devoid of pain, seem to recover the exploration phase. Collectively, *in vivo* studies highlighted that the analgesic effect is present in all the observed behaviors suggesting a central effect localized not only at the spinal level but also at supraspinal levels. Since the effect is present in both formalin phases, we hypothesize that analgesia blocks both the nociceptive input as well as the longer term effect induced by formalin injection. These data further support GluK1 partial agonists (such as **3**)[11] and antagonists (such as **7**)[11] as valuable option for the effective treatment of pain although with different behavioral outcomes.

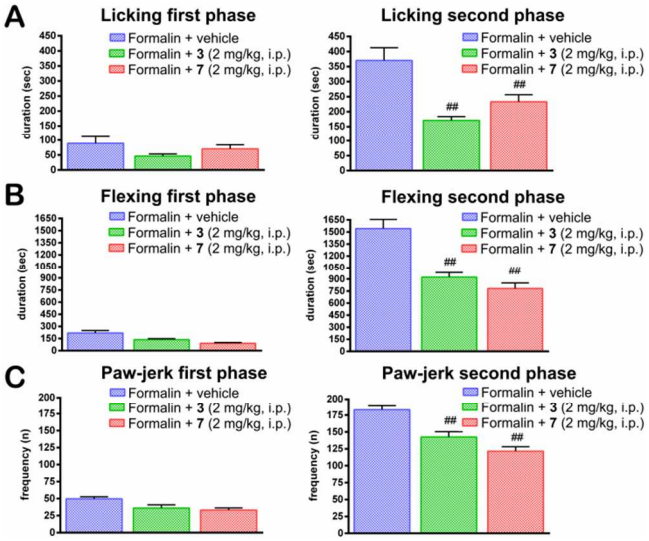

Figure 3. Behavioral responses to formalin injection (5%, 50 µL, dorsal paw), first (0-15') and second (15'-60') phases; animal experiments were conducted in compliance with institutional guidelines. Licking (A) and flexing (B) duration; (C) paw jerk frequency. #p<0.01, ##p<0.001 vs control.

Brain permeability of **7** was also evaluated using *in situ* rat brain perfusion technique. The obtained data showed that **7** can cross the rat BBB with a permeability of $5.9 \times 10^{-7} \pm 2.1 \times 10^{-7}$ cm/s (mean ± sem, $n = 3$). The low permeability was expected for a polar molecule like **7**. As high polarity of compounds is correlated with high unbound fraction and low distribution volume in the brain, effective concentration at the target site (brain extracellular compartment) of **7** can be achieved despite the low brain permeability.[25]

CONCLUSION

We further extended the structural and biological investigation of the class of pyrimidinediones structurally related to **1** as AMPA and KA receptors ligands. We described herein the synthesis, X-ray structural studies and biological evaluation of a new set of analogues **5a-c** and **6**. Specifically, we sought to explore focused bioisosteric replacements of the condensed heterocyclic moiety. Computational studies provided a rationalization of their binding properties. The new analogues **5a-c** preserved GluK1 affinity over GluA2 (for **5b,c**) with **5c** showing increased affinity for GluK3 (GluK3/GluK1 affinity ratio 6.0 for **5c**; and 625 for **2**). Brain permeability studies proved the capability of **7** to cross the BBB and, as GluK1 subtypes are involved in sensory transmission, the biological characterization of the series was continued assessing the analgesic potential in the formalin test of **3** and **7**. Both the antagonist **7** and the partial agonist **3** proved efficacy at 2 mg/kg, i.p. The present work provides further insights into the structural requirements for the design of AMPA receptor and KAR subtype selective ligands as well as additional evidences about the analgesic potential of GluK1/GluK3 ligands.

Experimental Section

Final compounds were analyzed by combustion analysis (CHN) to confirm purity >95%.

(*S*)-1-[2'-Amino-2'-carboxyethyl]-5,7-dihydrofuro[3,4-*d*]pyrimidine-2,4(1*H*,3*H*)-dione (5a). To a suspension of **13** (121 mg, 0.355 mmol) in dry DCM (10 mL), TFA (0.55 mL) was added dropwise at 0 °C and the mixture was stirred 4 h at rt. After evaporation, the crude was purified by ion-exchange resin (Dowex 50WX 8-400), using a 1:1 mixture of water/EtOH, then a 1% to 10% gradient of diluted NH_3 in water, to recover **5a** as a white solid (30 mg, 0.124 mmol, 35% yield). ^{1}H NMR (400 MHz, D_2O + DCl) δ 4.94 (t, J = 3.5 Hz, 2H), 4.79 (t, J = 3.5 Hz, 2H), 4.37-4.30 (m, 1H) 4.14-4.02 (m, 2H); ^{13}C NMR (100 MHz, D_2O + DCl) δ 168.9, 161.1, 154.8, 153.7, 109.1, 71.7, 71.0, 51.8, 46.0; ESI-MS *m/z* 242 $[M+H]^+$. Anal. ($C_9H_{11}N_3O_5$) C, H, N.

(*S*)-1-[2'-Amino-2'-carboxyethyl]-5,7-dihydropyrrolo[3,4-*d*]pyrimidin-2,4(1*H*,3*H*)-dione (5b). Starting from **19** (48 mg, 0.109 mmol) and as described for **5a**, title compound was obtained as white solid (21 mg, 0.087 mmol, 80% yield). ^{1}H NMR (300 MHz, D_2O) δ 4.27-4.08 (m, 1H), 4.02 (d, J = 6.0 Hz, 2H), 3.95-3.84 (m, 4H). ^{13}C NMR (75 MHz, D_2O) δ 172.4, 162.5, 156.7, 154.3, 110.2, 54.2, 50.7, 48.5, 47.6. ESI-MS *m/z* 241 $[M+H]^+$. Anal. ($C_9H_{12}N_4O_4$) C, H, N.

(*S*)-1-[2'-Amino-2'-carboxyethyl]-6-methyl-5,7-dihydropyrrolo[3,4-*d*]pyrimidin-2,4(1*H*,3*H*)-dione (5c). Starting from **22** (31 mg, 0.087 mmol) and as described for **5a**, title compound was obtained as white solid (11 mg, 0.043 mmol, 50% yield). ^{1}H NMR (300 MHz, D_2O) δ 4.09-3.95 (m, 4H), 3.89 (d, J = 5.1 Hz, 1H), 3.69 (s, 2H), 2.43 (s, 3H). ^{13}C NMR (75 MHz, D_2O) δ 171.4, 162.1, 155.5, 154.0, 109.4, 58.4, 56.2, 54.1, 47.1, 41.7. ESI-MS *m/z* 253 $[M-H]^-$. Anal. ($C_{10}H_{14}N_4O_4$) C, H, N.

(*S*)-1-[2'-Amino-2'-carboxyethyl]-3-((5-oxo-4,5-dihydro-1,3,4-oxadiazol-2-yl)methyl)thieno[3,4-

***d*]pyrimidine-2,4(1*H*,3*H*)-dione (6).** Starting from **26** (31 mg, 0.067 mmol) and as described for **5a**, title compound was obtained as white solid (10 mg, 0.34 mmol, 42% yield). ^{1}H NMR (300 MHz, D_2O) δ 8.18 (d, *J* = 3.2 Hz, 1H), 6.77 (d, *J* = 3.2 Hz, 1H), 4.59 (d, *J* = 2.3 Hz, 2H), 4.13-4.07 (m, 1H), 3.83-3.77 (m, 1H), 3.52-342 (m, 1H); ^{13}C NMR (300 MHz, D_2O) δ 171.8, 169.9, 162.3, 160.0, 151.8, 135.1, 131.6, 120.2, 104.5, 52.2, 50.7, 41.8. ESI-MS *m/z* 352 $[M-H]^-$. Anal. ($C_{12}H_{11}N_5O_6S$) C, H, N.

PDB ACCESSION CODES

6F29 (**2**) and 6F28 (**5c**). Authors will release the atomic coordinates and experimental data upon article publication.

ASSOCIATED CONTENT

Supporting Information. Experimental procedures, Figures and Tables for computational and X-ray studies and molecular formula strings. This material is available free of charge via the Internet at http://pubs.acs.org

AUTHOR INFORMATION

Corresponding Author

*Stefania Butini email: butini3@unisi.it; Giuseppe Campiani email: campiani@unisi.it
*For pharmacology, email: picker@sund.ku.dk
*For crystallography, email: jsk@sund.ku.dk

Author Contributions

The manuscript was written with contributions of all authors. All authors approved the final version of the manuscript.

Funding Sources

The Lundbeck Foundation (R.V., J.S.K.), GluTarget (R.V., L.H., K.F., J.S.K., D.S.P.), Danscatt (R.V., K.F., J.S.K).

ACKNOWLEDGMENT

We thank MAX-lab, Lund, Sweden for providing beamtime and beamline scientists for their help (R.V., K.F., J.S.K.). We thank Dr Andrew Orry (Molsoft LLC) for the trial license of ICM-Pro.

ABBREVIATIONS

AMPA, (*S*)-2-amino-3-(5-methyl-3-hydroxyisoxazol-4-yl)propanoic acid; BBB, blood-brain-barrier; DCM, dichloromethane; DMF, *N*,*N*-dimethylformamide; DMSO, dimethylsulfoxide; LBD, ligand-binding domain; iGluRs, ionotropic glutamate receptors; KARs, kainate receptors; *L*-Glu, *L*-glutamate; TFA, trifluoroacetic acid.

REFERENCES

1. Traynelis, S. F.; Wollmuth, L. P.; McBain, C. J.; Menniti, F. S.; Vance, K. M.; Ogden, K. K.; Hansen, K. B.; Yuan, H.; Myers, S. J.; Dingledine, R. Glutamate receptor ion channels: structure, regulation, and function. *Pharmacol. Rev.* **2010**, *62*, 405-496.
2. Pinheiro, P. S.; Perrais, D.; Coussen, F.; Barhanin, J.; Bettler, B.; Mann, J. R.; Malva, J. O.; Heinemann, S. F.; Mulle, C. GluR7 is an essential subunit of presynaptic kainate autoreceptors at hippocampal mossy fiber synapses. *Proc. Natl. Acad. Sci. U. S. A.* **2007**, *104*, 12181-12186.
3. Sobolevsky, A. I.; Rosconi, M. P.; Gouaux, E. X-ray structure, symmetry and mechanism of an AMPA-subtype glutamate receptor. *Nature* **2009**, *462*, 745-756.
4. Huettner, J. E. Kainate receptors and synaptic transmission. *Prog. Neurobiol.* **2003**, *70*, 387-407.
5. Jane, D. E.; Lodge, D.; Collingridge, G. L. Kainate receptors: pharmacology, function and therapeutic potential. *Neuropharmacology* **2009**, *56*, 90-113.
6. Lerma, J. Kainate receptor physiology. *Curr. Opin. Pharmacol.* **2006**, *6*, 89-97.
7. Matute, C. Therapeutic potential of kainate receptors. *CNS Neurosci. Ther.* **2011**, *17*, 661-669.
8. Bhangoo, S. K.; Swanson, G. T. Kainate receptor signaling in pain pathways. *Mol. Pharmacol.* **2013**, *83*, 307-315.
9. Campiani, G.; Morelli, E.; Nacci, V.; Fattorusso, C.; Ramunno, A.; Novellino, E.; Greenwood, J.; Liljefors, T.; Griffiths, R.; Sinclair, C.; Reavy, H.; Kristensen, A. S.; Pickering, D. S.; Schousboe, A.; Cagnotto, A.; Fumagalli, E.; Mennini, T. Characterization of the 1H-cyclopentapyrimidine-2,4(1H,3H)-dione derivative (S)-CPW399 as a novel, potent, and subtype-selective AMPA receptor full agonist with partial desensitization properties. *J. Med. Chem.* **2001**, *44*, 4501-4504.
10. Butini, S.; Pickering, D. S.; Morelli, E.; Coccone, S. S.; Trotta, F.; De Angelis, M.; Guarino, E.; Fiorini, I.; Campiani, G.; Novellino, E.; Schousboe, A.; Christensen, J. K.; Gemma, S. 1H-cyclopentapyrimidine-2,4(1H,3H)-dione-related ionotropic glutamate receptors ligands. structure-activity relationships and identification of potent and Selective iGluR5 modulators. *J. Med. Chem.* **2008**, *51*, 6614-6618.
11. Venskutonyte, R.; Butini, S.; Coccone, S. S.; Gemma, S.; Brindisi, M.; Kumar, V.; Guarino, E.; Maramai, S.; Valenti, S.; Amir, A.; Valades, E. A.; Frydenvang, K.; Kastrup, J. S.; Novellino, E.; Campiani, G.; Pickering, D. S. Selective kainate receptor (GluK1) ligands structurally based upon 1H-cyclopentapyrimidin-2,4(1H,3H)-dione: synthesis, molecular modeling, and pharmacological and biostructural characterization. *J. Med. Chem.* **2011**, *54*, 4793-4805.
12. Morelli, E.; Gemma, S.; Budriesi, R.; Campiani, G.; Novellino, E.; Fattorusso, C.; Catalanotti, B.; Coccone, S. S.; Ros, S.; Borrelli, G.; Persico, M.; Fiorini, I.; Nacci, V.; Ioan, P.; Chiarini, A.; Hamon, M.; Cagnotto, A.; Mennini, T.; Fracasso, C.; Colovic, M.; Caccia, S.; Butini, S. Specific targeting of peripheral serotonin 5-HT(3) receptors. Synthesis, biological investigation, and structure-activity relationships. *J Med Chem* **2009**, *52*, 3548-3562.
13. Schönbrunn, E.; Lawrence, N. J.; Lawrence, H. R. Potent Dual Brd4-kinase Inhibitors as Cancer Therapeutics. WO 2016022460 A1, Feb 11, 2016.
14. Chavan, S. P.; Dhawane, A. N.; Kalkote, U. R. Tandem Aza-Michael-Condensation-Aldol Cyclization Reaction: Approach to the Construction of DE Synthon of (+/-)-Camptothecin. *Synlett.* **2008**, *18*, 2781-2784.
15. Simpson, G. L.; Gordon, A. H.; Lindsay, D. M.; Promsawan, N.; Crump, M. P.; Mulholland, K.; Hayter, B. R.; Gallagher, T. Glycosylated foldamers to probe the carbohydrate-carbohydrate interaction. *J. Am. Chem. Soc.* **2006**, *128*, 10638-10639.
16. Hayward, S.; Berendsen, H. J. Systematic analysis of domain motions in proteins from conformational change: new results on citrate synthase and T4 lysozyme. *Proteins* **1998**, *30*, 144-154.
17. Mollerud, S.; Frydenvang, K.; Pickering, D. S.; Kastrup, J. S. Lessons from crystal structures of kainate receptors. *Neuropharmacology* **2017**, *112*, 16-28.
18. Venskutonyte, R.; Frydenvang, K.; Gajhede, M.; Bunch, L.; Pickering, D. S.; Kastrup, J. S. Binding site and interlobe interactions of the ionotropic glutamate receptor GluK3 ligand binding domain revealed by high resolution crystal structure in complex with (S)-glutamate. *J. Struct. Biol.* **2011**, *176*, 307-314.
19. Veran, J.; Kumar, J.; Pinheiro, P. S.; Athane, A.; Mayer, M. L.; Perrais, D.; Mulle, C. Zinc potentiates GluK3 glutamate receptor function by stabilizing the ligand binding domain dimer interface. *Neuron* **2012**, *76*, 565-578.
20. Venskutonyte, R.; Frydenvang, K.; Hald, H.; Rabassa, A. C.; Gajhede, M.; Ahring, P. K.; Kastrup, J. S. Kainate induces various domain closures in AMPA and kainate receptors. *Neurochem. Int.* **2012**, *61*, 536-545.
21. Mayer, M. L. Crystal structures of the GluR5 and GluR6 ligand binding cores: molecular mechanisms underlying kainate receptor selectivity. *Neuron* **2005**, *45*, 539-552.
22. Vistoli, G.; Mazzolari, A.; Testa, B.; Pedretti, A. Binding space concept: a new approach to enhance the reliability of docking scores and its application to predicting butyrylcholinesterase hydrolytic activity. *J. Chem. Inf. Model.* **2017**, *57*, 1691-1702.
23. Maicheen, C.; Phosrithong, N.; Ungwitayatorn, J. Biological activity evaluation and molecular docking study of chromone derivatives as cyclooxygenase-2 inhibitors. *Med. Chem. Res.* **2017**, *26*, 662-671.
24. Capone, F.; Aloisi, A. M. Refinement of pain evaluation techniques. The formalin test. *Ann. Ist. Super. Sanita* **2004**, *40*, 223-229.
25. Gynther, M.; Petsalo, A.; Hansen, S. H.; Bunch, L.; Pickering, D. S. Blood-brain barrier permeability and brain uptake mechanism of kainic acid and dihydrokainic acid. *Neurochem Res* **2015**, *40*, 542-549.

SYNOPSIS TOC